Title

The role of wind gusts in upper ocean diurnal variability

Journal

Journal of Geophysical Research: Oceans, 122(9)

ISSN

2169-9275

Authors

Giglio, D
Gille, ST
Subramanian, AC
et al.

Publication Date

2017-09-01

DOI

10.1002/2017JC012794

Peer reviewed

AGU PUBLICATIONS

JGR

Journal of Geophysical Research: Oceans

RESEARCH ARTICLE

10.1002/2017JC012794

The role of wind gusts in upper ocean diurnal variability

Donata Giglio[1], Sarah T. Gille[1], Aneesh C. Subramanian[2], and San Nguyen[1]

[1]Scripps Institution of Oceanography, University of California San Diego, La Jolla, California, USA, [2]Department of Physics, University of Oxford, Oxford, UK

Key Points:
- Except during nighttime convection, wind gusts regulate how fast surface water is mixed to greater depths when daily mean winds are weak
- Diurnal winds are weaker in amplitude than wind gusts and play a minor role in upper ocean mixing
- A 1-D process model yields a good estimate of observed upper ocean diurnal temperature, even with stochastic wind gusts as input

Correspondence to:
D. Giglio,
dgiglio@ucsd.edu

Citation:
Giglio, D., S. T. Gille, A. C. Subramanian, and S. Nguyen (2017), The role of wind gusts in upper ocean diurnal variability, *J. Geophys. Res. Oceans*, *122*, 7751–7764, doi:10.1002/2017JC012794.

Received 13 FEB 2017
Accepted 20 JUL 2017
Accepted article online 24 JUL 2017
Published online 26 SEP 2017

Abstract Upper ocean processes play a key role in air-sea coupling, with variability on both short and long time scales. The diurnal cycle associated with diurnal solar insolation and nighttime cooling, may act, along with stochastic wind variability, on upper ocean temperatures and stratification resulting in a diurnal warm layer and a nonlinear rectified effect on longer time scales. This study describes diurnal changes in upper ocean temperature for a location in the equatorial Indian Ocean, using observations from the Dynamics of the Madden-Julian Oscillation field campaign, a high vertical resolution 1-D process model, and a diurnal cycling scheme. Solar forcing is the main driver of diurnal variability in upper ocean temperature and stratification. Yet except during nighttime convection, winds with variability on the order of hours (here referred to as "wind gusts") regulate how fast surface water is mixed to greater depths when daily mean winds are weak. Wind gusts are much stronger than diurnal winds. Even using stochastic wind gusts but no diurnal winds as input in a 1-D process model yields an estimate of diurnal temperature that compares well with observations. A new version of the Large and Caron (2015) scheme (LC2015) provides an estimate of upper ocean diurnal temperature that is consistent with observations. LC2015 has the advantage of being suitable for implementation in a climate model, with the goal to improve SST estimates, hence the simulated heat flux at the air-sea interface. Yet LC2015 is not very sensitive to the inclusion or omission of the high-frequency component of the wind.

1. Introduction

Diurnal changes in upper ocean temperature and stratification are primarily driven by diurnal solar insolation and nighttime cooling [*Wade et al*., 2011]. Yet nonsolar surface heat flux, wind and buoyancy driven mixing, and stratification in the upper few meters of the ocean regulate the transfer of heat to greater depths in time [*Schudlich and Price*, 1992; *Soloviev and Lukas*, 2006; *Cronin and Kessler*, 2009; *Matthews et al*., 2014]. Both diurnal winds and higher frequency components of the wind may play a role in regulating the diurnal cycle in the upper ocean. The resulting near-surface diurnal warming is usually less than 1°C [*Gille*, 2012; *Sutherland et al*., 2016] at 5 dbar but can be more than 3°C at 0.6 m, in conditions of weak winds and strong cloud-free insolation [*Stramma et al*., 1986; *Prytherch et al*., 2013].

Temperature variability at the air-sea interface drives exchanges of heat and water vapor between the atmosphere and the ocean, making near-surface diurnal warming an important process in the climate system [*Bernie et al*., 2005; *Danabasoglu et al*., 2006; *Bernie et al*., 2007; *Kawai and Wada*, 2007; *Bernie et al*., 2008]. Near-surface diurnal warming impacts large-scale variability in the tropics (e.g., intraseasonal time scales) [*Bernie et al*., 2007; *Seo et al*., 2014; *Ruppert and Johnson*, 2014], as well as long-term mean fields. The daily mean Sea Surface Temperature (SST) anomaly due to the diurnal warm layer increases long-term mean SST [*Bernie et al*., 2008; *Weller et al*., 2014], and accounting for it in a model simulation improves mean precipitation [*Bernie et al*., 2008]. Also, the daily mean SST anomaly due to the diurnal warm layer drives an anomalous heat flux at the air-sea interface. Neglecting this process in a coupled ocean-atmosphere model would incur an erroneous flux ($\sim$4 W m^{-2}), warming the ocean and cooling the atmosphere [*Matthews et al*., 2014].

Diurnal cycling schemes have been designed to represent diurnal warming in climate models [*Zeng and Beljaars*, 2005; *Large and Caron*, 2015], without the prohibitive costs [*Bernie et al*., 2005, 2007, 2008] associated with high vertical (and high temporal) resolution. Building on the pioneering effort of *Zeng and Beljaars* [2005], *Large and Caron* [2015] introduced a diurnal cycling scheme with improved physics, including

shallow stable boundary layers, as well as diurnal cycles of salinity and ocean currents. This parameterization estimates the temperature difference between the air-sea interface and the shallowest ocean level of a global Coupled General Circulation Model (CGCM), often deeper than a few meters and (inaccurately, e.g., *Fairall et al*. [1996]) used as surface temperature relevant for heat and moisture fluxes in air-sea interactions [*Zeng and Beljaars*, 2005]. *Large and Caron* [2015] implement their diurnal cycling scheme in the Community Earth System Model (CESM) and suggest a diurnal warming generally of order a few degrees Celsius between 40°S and 60°N, consistent with *Bernie et al*. [2005]. The impact of the diurnal cycling scheme on nonsolar air-sea heat flux is not large (i.e., generally less than 5 W m^{-2}, while nonsolar fluxes are typically of order 100 W m^{-2} and uncertainties greater than 10 W m^{-2}), except in the equatorial Pacific cold tongue [*Large and Caron*, 2015]. Also, precipitation biases in the CESM are attributed to inadequate model representation of relevant physical processes (e.g., convection) rather than the diurnal cycle of SST [*Large and Caron*, 2015]. Yet applying the *Large and Caron* [2015] parametrization may have a larger impact on either the diurnal cycle of precipitation or precipitation frequency as this physics is improved.

The present work aims for a better process understanding of upper ocean diurnal variability. One focus is the impact, on upper ocean mixing, of diurnal winds versus winds with variability on the order of hours (referred to as "wind gusts" in the following). We use observations from the Dynamics of the Madden-Julian Oscillation (DYNAMO) field campaign, at a site in the equatorial Indian Ocean, and a one-dimensional water column model (i.e., General Ocean Turbulence Model, GOTM). We also investigate how the *Large and Caron* [2015] scheme represents key air-sea interactions.

Sections 2, 3, and 4 describe method, data, and models, respectively. Section 5 presents results from observations (5.1), GOTM (5.2), and *Large and Caron* [2015] (5.3), with the impact of diurnal winds versus wind gusts on upper ocean diurnal temperature described in section 5.2. A summary and concluding remarks are in section 6.

2. Method

We describe upper ocean diurnal temperature changes in terms of T_W (Figure 1), the difference between a temperature value below the sea surface (T_{bulk}, here at 5 cm) and a foundation temperature (T_f, here at 10 m). T_W is the metric of choice since it provides the information to estimate SST in climate models (where the shallowest ocean level is around 10 m), and hence to improve the simulated heat flux at the air-sea interface. Temperature at the air-sea interface can in fact be expressed as $T_{skin} = T_f + T_W + T_C$, with T_C the cool skin effect [*Fairall et al*., 1996]. For instance, *Large and Caron* [2015] estimate T_W and T_C from atmospheric forcing, assuming a mixing regime in the upper ocean that varies during the day [*Large and Caron*, 2015]. We also compare model results with observations in the diurnal warm layer at 5 cm, 1 m, and 5 m, where measurements are available.

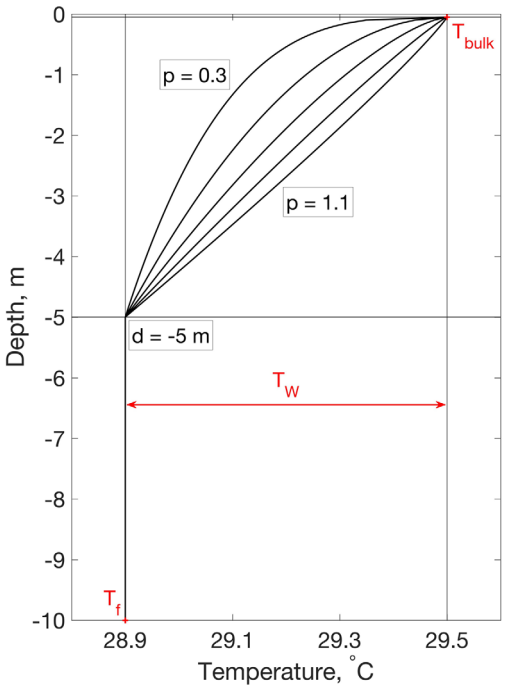

Figure 1. Schematic for the functional form describing the vertical temperature profile in *Large and Caron* [2015]. Values of the *d* and *p* parameters used in this analysis are included, along with annotations for T_{bulk}, T_f, and T_W.

In this study, the nomenclature for different near-surface temperatures does not follow the recommendations by *Donlon et al*. [2007]. *Donlon et al*. [2007] distinguish temperature at the air-sea interface, and skin, subskin, depth and foundation temperature, with the assumption that the foundation temperature does not show any diurnal variability. Because of the multitude of different temperature depths, *Donlon et al*. [2007] recommend that a depth temperature should be qualified by the measurement depth (i.e., T_{5cm}) rather than using the generic term T_{bulk}. Here we follow the definitions employed by *Large and Caron* [2015], and we

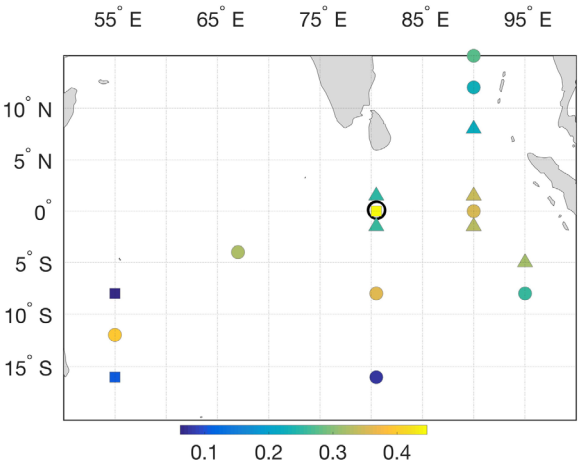

Figure 2. Maximum $T_{W_{RAMA}}$ (°C, color) during a climatological day, from RAMA moorings in the Indian Ocean. Near-surface temperature observations are collected at a depth of 1 m for most of the moorings, except two sites which measure at 1.5 m depth (i.e., 1.5°S, 90°E and 5°S, 95°E). Daily climatologies are estimated from observations during September 2012 to April 2013 (dots), October 2007 to May 2008 (triangles), and 11–21 October 2011 (squares, i.e., Period O in this analysis). The black circle on the Equator indicates the approximate location of DYNAMO leg-2 and leg-3 of the R/V Revelle.

consider both T_{bulk} and T_f as depth temperatures (as defined in *Donlon et al.* [2007]) and specify their measurement depth.

Finally, we use the term "wind gusts" to indicate winds with variability on time scales of the order of hours. This nomenclature differs from that of the National Weather Service, the American Meteorological Society, and the World Meteorological Organization who formally define gusts to be shorter extreme events.

3. Observations

3.1. DYNAMO Campaign

The DYNAMO observation campaign focused on measuring the environmental conditions that initiate the Madden-Julian Oscillation (MJO) cycle [*Yoneyama et al.*, 2013]. As part of the DYNAMO campaign (late 2011 to early 2012), observations of near-surface ocean temperature, 10 m winds, heat and freshwater fluxes at the air-sea interface were collected, with a 1 min sampling interval, around 0°N, 80.5°E (Figure 2, black circle), on research cruises aboard the R/V Revelle. In the following, we analyze two time periods: 11–21 October 2011 (during leg 2, henceforth Period O), and 13–22 November 2011 (during leg 3, henceforth Period N). The estimate of T_W relies on near-surface temperature measurements (i.e., T_{bulk}) from sea-snake floating thermistors at a depth of 5 cm. T_f is taken as temperature at 10 m depth from the Chameleon turbulence profiler [*Moum et al.*, 1995].

3.2. RAMA Moorings

The Research Moored Array for African-Asian-Australian Monsoon Analysis and Prediction (RAMA) was designed to study the Indian Ocean's role in the monsoons [*McPhaden et al.*, 2009]. In this analysis, we use RAMA mooring observations (Figure 2) of upper ocean temperature at 1, 5, and 10 m, except for two sites where the shallowest measurement is at 1.5 m depth (i.e., 1.5°S, 90°E and 5°S, 95°E). A 1–1.5 m depth for near-surface temperature makes the estimate of T_W from RAMA moorings (i.e., $T_{W_{RAMA}}$) not directly comparable to T_W from DYNAMO observations or model output presented in this study. However, $T_{W_{RAMA}}$ has the advantage of being available at 0°N, 80.5°E for a longer time period, from 9 August 2008 to 23 November 2011 (with a gap around October 2010 to August 2011), overlapping with Period O and Period N.

4. Models

4.1. GOTM

The General Ocean Turbulence Model (GOTM) [*Burchard et al.*, 1999] is one-dimensional and has been successfully used to reproduce diurnal variability [*Hallsworth*, 2005; *Pimentel et al.*, 2008a,2008b; *Karagali et al.*, 2017]. GOTM implements different types and levels of closure models to compute vertical turbulent fluxes. In this study, we use a two-equation closure model and dynamic formulations of both turbulent kinetic energy (k) and rate of dissipation. GOTM also estimates downward irradiance at different ocean depths, $I(z)$, following *Paulson and Simpson* [1977], i.e., $\frac{I(z)}{I_0} = Ae^{\frac{z}{\eta_1}} + (1-A)e^{\frac{z}{\eta_2}}$, with I_0 the solar radiation. In our simulations, $A = 0.58$, $\eta_1 = 0.35$, and $\eta_2 = 23$, consistent with water type I as classified by *Jerlov* [1968] and with clear water conditions in the region [*Li et al.*, 2012; *Matthews et al.*, 2014; *Strutton et al.*, 2015]. Clear water conditions were observed during the period of interest by a glider at 80°E, between 3°S and 4°S [*Webber et al.*, 2014, Figure 7c], with the mean 0–10 m chlorophyll concentration less than 1 mg m^{-3}. Yet *Karagali et al.* [2017]

Table 1. How T_W From Different GOTM and LC2015 Experiments Compares to Observations: Correlation With Measured Values (r) and Root-Mean-Square (rms, °C) Difference, Computed Only for $T_W \geq 0$ (This Is Always the Case in *Large and Caron* [2015])

	T_{bulk}	T_f	10 m Winds	T_W, Oct		T_W, Nov	
				r	rms	r	rms
GOTM $\Delta z=10$ cm $\Delta t=5$ min	At 5 cm	At 10 m	G1. Observed	0.9	0.23	0.86	0.35
			G1. Observed				
			G2. 24 h smoothed	0.86	0.31	0.76	0.63
			G3. G2 + diurnal	0.86	0.3	0.75	0.59
			G4. G2 + stochastic gusts	0.87	0.18	0.81	0.36
			G5. G2 w/nonsolar heating from smoothed wind	0.78	0.55	0.64	1.08
LC2015 parameterization $\Delta t=5$ min	*only* T_W estimate		L1. Observed	0.91	0.15	0.86	0.39
			L2. 24 h smoothed	0.89	0.17	0.82	0.42
			L3. L1, LC15_stnd	0.87	0.19	0.71	0.52

show (for different sites) that a nine band solar absorption model performs better than the standard two band scheme in GOTM simulations of diurnal SST.

GOTM experiments are performed here with 10 cm vertical resolution and a 5 min time step. In the following, test cases with finer resolution are not discussed, since they yield similar results. The shallowest level resolved is at 5 cm, and temperature at this depth is used as an estimate for T_{bulk}. The output temperature at 10 m is designated as T_f. Atmospheric forcing for the simulations is from shipboard DYNAMO observations (for Period O and Period N), and includes short-wave and long-wave radiation, latent and sensible heat, precipitation, evaporation, and zonal and meridional momentum fluxes.

We use GOTM to model upper ocean variability, and to understand vertical processes relevant for the observed diurnal cycle (e.g., mixing). We investigate the role of wind gusts (i.e., winds with variability on time scales of the order of hours) versus diurnal and lower frequency variability (in winds), changing the wind forcing in input, while other air-sea fluxes stay the same (i.e., are set to the observed values) or are consistent with modified winds. We perform a set of experiments (Table 1):

G1. Using the observed zonal and meridional winds at 10 m.
G2. Smoothing the observed winds in time with a 24 h window, while other air-sea fluxes stay the same (i.e., nonsolar heating estimated from observed winds).
G3. As G2, but including the observed diurnal winds.
G4. As G2, but including stochastic wind gusts.
G5. As G2, but estimating nonsolar heating from smoothed winds.

In scenario G4, stochastic wind gusts (g_t, at time step t) are computed as red noise (i.e., $g_{t+1}=r_1\, g_t+(1+r_1^2)^{1/2}\, w_{t+1}$, $t \geq 1$) starting from Gaussian white noise (w) with the same standard deviation (σ^{obs}) as the observed wind gusts (g_t^{obs}), and the observed leg-1 correlation coefficient (r_1) of g_{t+1}^{obs} and g_t^{obs}. Experiment G4 is run for an ensemble of 1000 members, and the ensemble mean and standard deviation are shown.

4.2. A Diurnal Cycling Scheme by *Large and Caron* [2015]

A detailed description of the diurnal cycling scheme can be found in *Large and Caron* [2015], along with its implementation in a climate model (their Appendix A). At each time step of a climate model run, the diurnal cycling scheme provides an estimate of the difference between T_{skin} (and T_{bulk}) and temperature at the shallowest ocean level of the model (e.g., T_f at 10 m), allowing for a better estimate of air-sea fluxes. The estimate for the evolution of $T_W(=T_{bulk}-T_f)$ assumes a functional form $T(z)$ for the temperature profile in the upper ocean. $T(z)=T_{bulk}-\left[\frac{(z+\delta)}{(-d+\delta)}\right]^p T^W$ [*Large and Caron*, 2015, equation (6)], with $z<0$, δ the depth relevant for the cool skin effect (i.e., order of millimeters) [*Fairall et al.*, 1996], $T(-\delta)=T^{bulk}$, and p and d parameters that define the structure of $T(z)$ for $\delta < -z < d$ (Figure 1). From depth d to the foundation level (i.e., where $T = T^f$), T is assumed constant (Figure 1). In the following, $d=5$ m and $p=0.3$ based on observations.

The evolution of T_W in time is based on the atmospheric forcing [*Large and Caron*, 2015, equation (10)], i.e., $\partial_t T_W=H_d\frac{(p+1)}{pd}-K_d T_W\frac{(p+1)}{d^2}$, where H_d is effective heating, and K_d sub-grid-scale turbulent diffusivity. H_d includes the contribution of solar and nonsolar surface heat flux, with a parameterization for solar

absorption that is consistent with clear water conditions and the GOTM experiments described in section 4.1. In the following, the estimate of K_d considers three ocean boundary layer regimes: (I) well mixed, (III) shallow stable, and (IV) deepening convective. The original *Large and Caron* [2015] scheme also includes a deep stable regime (i.e., Regime II), which does not occur often in low wind and high solar forcing days (when the diurnal T_W is larger) and is omitted here for simplicity. The simplification is an advantage, especially from the perspective of implementing the scheme in climate models [*Large and Caron*, 2015]. During Regime I, the upper ocean is well mixed, and $T_W=0$ (i.e., the buoyancy forcing is convective). Regime III starts as the effective buoyancy forcing becomes stable and is characterized by a contribution to K_d from internal waves ($\kappa_o=0.2$ cm^2 s^{-1}), plus a shear-driven mixing that scales with a much larger mixing coefficient (ν_o of order 0.4 cm^2 s^{-1}), i.e., $K_d=\kappa_o+\nu_o[1+C_A(\frac{Ri_d}{Ri_0})^{\gamma}]^{-1}$, with Ri_d a gradient Richardson number [*Large and Caron*, 2015, equations (20) and (17)]. In the following, $Ri_0=1$, $C_A=0.67$, and $\gamma=0.6$. Most of the daytime is in Regime III, consistent with favorable conditions for shear-driven mixing [*Sutherland et al*., 2016; *Smyth et al*., 2013]. When Regime IV takes over, it produces a strong relaxation of T_W back to zero (with K_d proportional to the friction velocity) [*Large and Caron*, 2015, equation (18)], unless this limit has already been reached. Finally, when the estimate for T_W would become negative, Regime I is reinstated. Negative values for T_W may occur in observations (e.g., during precipitation events) but are not represented in the diurnal cycling scheme. In the standard version of the *Large and Caron* [2015] scheme (i.e., LC15_stnd in the following), the transition from Regime III to Regime IV occurs when the effective buoyancy forcing becomes unstable. In the variant version of the parametrization, here identified as LC2015, the transition to Regime IV by the standard criteria is delayed until a bulk Richardson number [*Large and Caron*, 2015, equation (13)] falls below a critical value ($Ri_{cr}=0.3$ here), in order to avoid a too rapid relaxation of T_W back to zero and to achieve a better representation of the observed process, as suggested by *Large and Caron* [2015].

As with GOTM, we investigate the role of wind gusts versus low-frequency variability (in winds), changing the wind forcing in input to the parameterization, while other air-sea fluxes stay the same (i.e., are set to the observed values). We perform a set of experiments with a 5 min time step (Table 1):

L1. Using the observed zonal and meridional winds at 10 m.
L2. Smoothing the observed winds in time with a 24 h window.
L3. As L1, but for LC15_stnd.

5. Results

In this section, we describe the observed T_W (section 5.1), along with estimates from GOTM (section 5.2) and LC2015 (section 5.3).

Estimates of T_W from different GOTM and LC2015 experiments are compared to observations, computing correlation (r) with measured values and root-mean-square (*rms*, °C) difference. Table 1 shows r and *rms* values for the different cases considered here.

5.1. Observed T_W

The diurnal peak in $T_{W_{RAMA}}$ for a composite day varies with location in the tropical Indian Ocean (Figure 2, comparing markers of the same shape with one another), with the timing of the peak between hour 1400 and hour 1600 Local Solar Time (LST). In addition, the diurnal peak at a given site changes in time (not shown), as atmospheric forcing, local dynamics, and chlorophyll concentration (water clarity) in the upper ocean modulate the structure of near-surface diurnal warming [*Soloviev and Lukas*, 2006; *Matthews et al*., 2014].

A composite day of $T_{W_{RAMA}}$ at 0°N, 80.5°E, during Period O and Period N (Figure 3, dashed red line), is characterized by a peak between hour 1500 and hour 1600 LST, consistent with diurnal variability in temperature at 0.5 m based on Seaglider data (78.83°E, 1.5°S–4°S) [*Matthews et al*., 2014]. Due to day-to-day variations of the diurnal warm layer, compositing over a longer time period (Figure 3, dotted red line) results in a slightly different phasing, and a smaller peak amplitude instead. In general, during the DYNAMO field experiment, a diurnal warm layer develops on those days when the solar radiation flux is high (above 80 W m^{-2}) and the wind speed is low (below 6 m s^{-1}) [*Matthews et al*., 2014], with higher occurrence when the convectively suppressed phase of the MJO is underway [*Moum et al*., 2013; *Matthews et al*., 2014]. Period O and Period N are characterized by such conditions on most days.

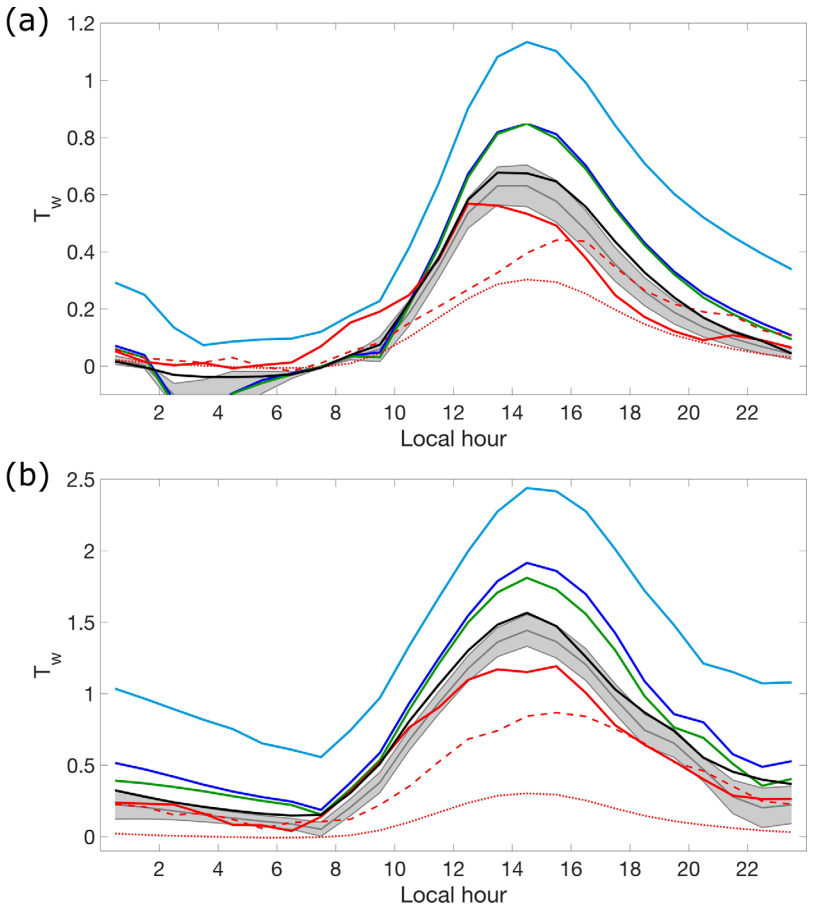

Figure 3. Composite day for T_W (°C) during (a) Period O and (b) Period N. T_W is from DYNAMO R/V Revelle observations (red line), GOTM experiment G1 (black), G2 (blue), G3 (green), G4 (gray), and G5 (light blue). For experiment G4, the gray line is the ensemble mean and the shade is the standard deviation. A composite day for $T_{W_{RAMA}}$ is shown for the same time periods (dashed red line) and for all the observations available at the 0°N, 80.5°E RAMA mooring (dotted red line).

During Period O and Period N, DYNAMO observations from the R/V Revelle show a peak in T_W around 1400 LST (Figure 3, solid red line), consistent with near-surface diurnal variability from previous studies [e.g., *Price et al*., 1986; *Schudlich and Price*, 1992; *Fairall et al*., 1996; *Wade et al*., 2011; *Prytherch et al*., 2013; *Large and Caron*, 2015]. The 1400 LST peak is earlier than the diurnal peak in $T_{W_{RAMA}}$. T_{bulk} from DYNAMO sea-snake floating thermistors is measured at 5 cm, while T_{bulk} used to compute $T_{W_{RAMA}}$ is at 1 m (section 3); hence, the difference in phasing between T_W and $T_{W_{RAMA}}$ is consistent with the hypothesis that surface water that is warmed by solar radiation is mixed to progressively deeper depths over the course of several hours [*Cronin and Kessler*, 2009; *Smyth et al*., 2013; *Sutherland et al*., 2016]. T_W is small overnight and starts increasing after 0006 LST (Figure 3), as the sun rises. A diurnal warm layer forms, and the resulting stratification traps air-sea momentum flux, with the development of a shear flow [*Smyth et al*., 2013]. The net surface energy flux (i.e., solar plus nonsolar heating) diminishes in the afternoon, and shear instabilities entrain fluid below the diurnal layer, transferring both heat and kinetic energy downward [*Smyth et al*., 2013; *Sutherland et al*., 2016]. The near-surface ocean starts cooling around 1400 LST, T_W decreases (Figure 3), and convective cooling eventually mixes upper ocean temperatures deeper. The peak T_W is larger for days of high solar radiation and low wind (Figures 4 and 5), consistent with *Matthews et al*. [2014] and *Moum et al*. [2013], and no significant diurnal cycle in T_W is observed on 13 October, 19 October (Figure 4), or 22 November (Figure 5) 2011, when SW_0 is small and the wind stress amplitude relatively large. Overall, the peak amplitude for a composite day is larger (by a factor of about 2) for Period N (~1.15°C) compared to Period O (~0.55°C, Figure 3), consistent with a stronger incoming solar radiation and a smaller median wind stress amplitude during Period N.

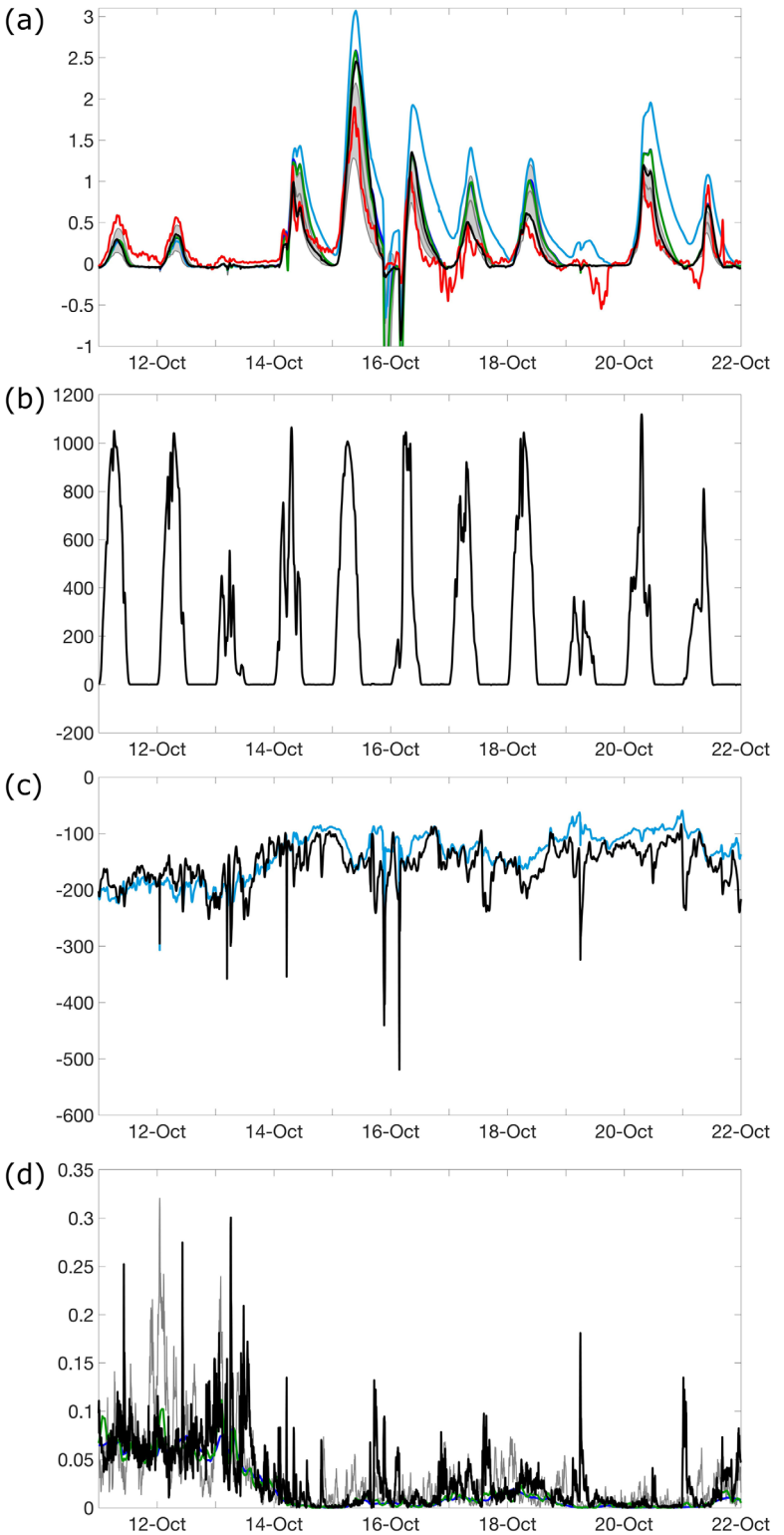

Figure 4. Period O time series of (a) T_W (°C), and (b) observed solar radiation (W m^{-2}), (c) nonsolar heating (W m^{-2}), and (d) wind stress amplitude (kg m^{-1} s^{-2}) at the air-sea interface. In Figure 4a, T_W is from DYNAMO R/V Revelle observations (red line), GOTM experiment G1 (black), G2 (blue), G3 (green), G4 (gray, as in Figure 3), and G5 (light blue). In Figure 4c, the nonsolar heating is from observed (black line), and 24 h smoothed (light blue) wind forcing. In Figure 4d, the wind stress amplitude is from observed (black line), 24 h smoothed (blue), and 24 h smoothed plus diurnal (green) wind forcing. One of the ensemble members of experiment G4 is also shown (gray line). Tick marks on the horizontal axis correspond to 0500 LST for each day.

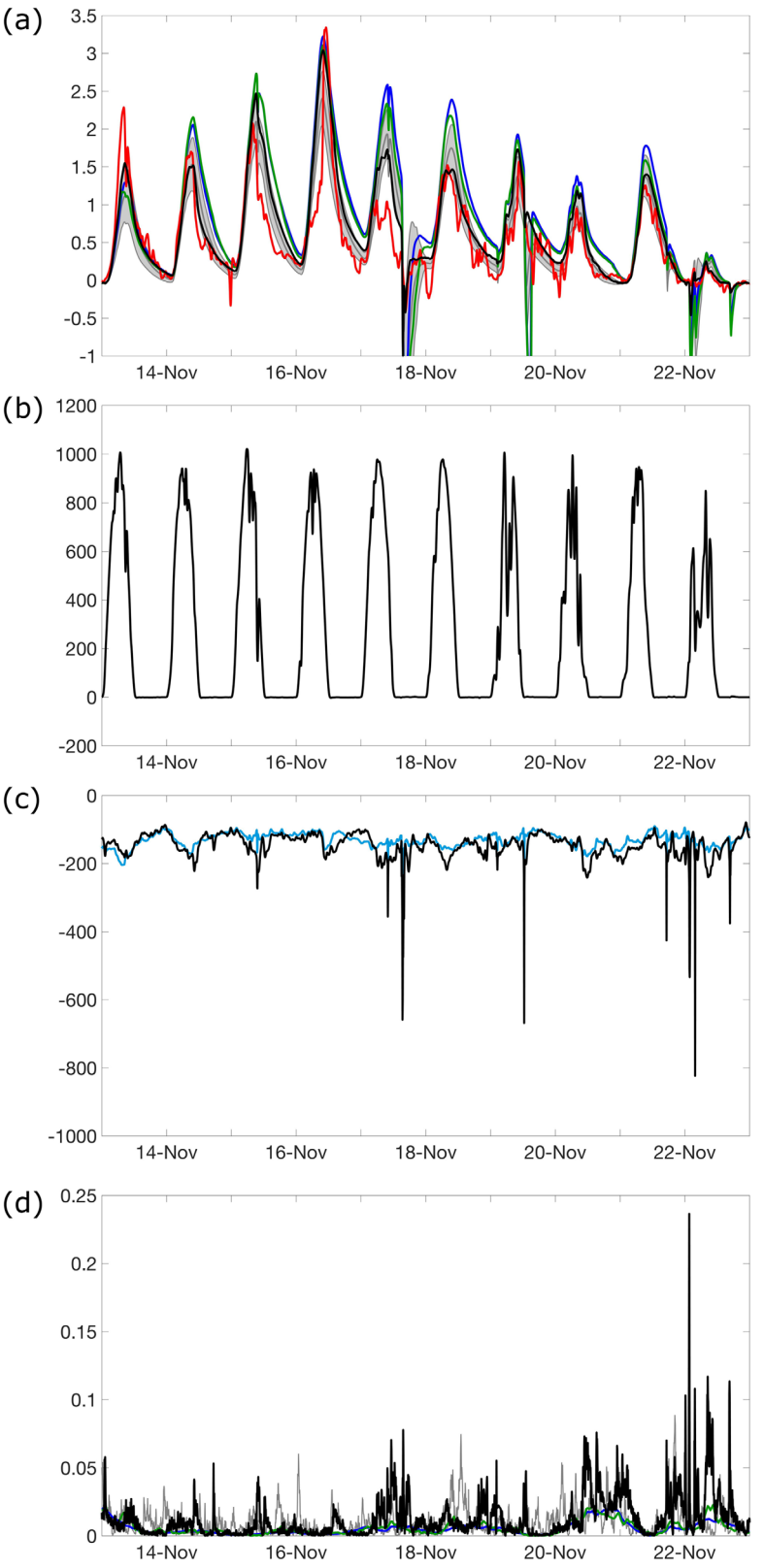

Figure 5. Same as Figure 4, but for Period N and not showing experiment G5 in (a).

5.2. T_W From GOTM

The estimate of T_W from GOTM using the observed winds as input to the model (experiment G1, $T_{W_{G1}}$; Figures 4d–5d, black line), compares well with observations for both periods of interest here (Figures 3, 4a, and 5a, black line), with a correlation coefficient $r = 0.9$, $rms = 0.23$°C for Period O, and $r = 0.86$, $rms = 0.35$°C for Period N (Table 1). For a few days (e.g., 15 October and 17 November), the diurnal peak T_W from GOTM is 0.5°C larger than observations, and the difference may suggest a role of horizontal advection processes (not represented in GOTM).

If winds input to GOTM are smoothed in time with a 24 h window (experiment G2; Figures 4d–5d, blue line), the vertical structure of mixing (hence temperature) is different from experiment G1 (not shown), and $T_{W_{G2}}$ is further from observations (blue versus red line in Figures 3, 4a, and 5a). Smoothing the winds for experiment G2 suppresses high-frequency winds with variability on time scales of the order of hours and amplitude up to $\sim$8 m s^{-1} larger than the daily mean wind (Figures 4d and 5d). These wind gusts may be associated with boundary layer large eddies, convective precipitation, and convective cloudiness [*Zeng et al*., 2002], and discarding them results in reduced mixing, hence a slower transmission of surface water to greater depths, during weak daily mean wind conditions. Consequently, T_W increases faster as the sun rises, the maximum T_W during the day is greater, and the cooling phase may be slower (Figures 3, 4a, and 5a). In experiment G2, the daily peak in T_W for the composite day is $\sim$0.3°C larger than in G1. The difference between $T_{W_{G2}}$ and $T_{W_{G1}}$ reduces slowly during the cooling phase of T_W (Figure 3), with G2 yielding $rms = 0.31$°C for Period O and $rms = 0.63$°C for Period N (Table 1). Yet the correlation between $T_{W_{G2}}$ and the observed T_W is still good, consistent with solar forcing playing the leading role in regulating T_W diurnal variability [*Wade et al*., 2011].

Adding the observed (small) diurnal variability to the 24 h smoothed wind forcing (experiment G3; Figures 4d and 5d, green line) only slightly improves on the output from experiment G2 (green versus blue line in Figures 3, 4a, and 5a). A clear improvement on experiment G2, results from adding stochastic wind gusts to the 24 h smoothed wind forcing (experiment G4, section 4.1; Figures 4d and 5d, gray line for one of the 1000 ensemble members). The estimate of $T_{W_{G4}}$ compares well to observations (gray versus red line in Figures 3, 4a, and 5a), with $r = 0.87$, $rms = 0.18$°C for the ensemble mean in Period O, and $r = 0.81$ and $rms = 0.36$°C in Period N (Table 1).

Finally, using the same (24 h smoothed) wind forcing as G2, but now to estimate both momentum fluxes and nonsolar heat flux input to GOTM (experiment G5; Figures 4c–5c, light blue line) yields the estimate of T_W (i.e., $T_{W_{G5}}$) that is furthest from observations (Figures 3 and 4a), indicating that wind gusts have a stronger impact on the amplitude of diurnal temperature through changes they introduce in nonsolar heating than through changes in upper ocean mixing. Yet upper ocean mixing regulates the timing of the diurnal peak at different depths, which is (similarly) later than observations for both experiments G5 and G2 (Figures 6a and 6b, top).

Overall, GOTM experiment G1 estimates most of the variability at 5 cm (not shown) and 1 m, as well as some of the diurnal signal at 5 m (Figure 6c), which is weak for most days of interest here and does not emerge in the composites (Figures 6a and 6b, bottom). The best comparison with observed diurnal variability at 5 m is during those days with stronger daily mean winds (e.g., 11–12 October in Figure 6c), when the effect of wind gusts is not prominent (Figure 4a). GOTM may be missing some of the dynamics that are relevant in weak daily mean wind conditions (e.g., dynamics related to surface waves or horizontal and vertical advection) and/or wind gusts present in the input fields are weaker than real wind gusts. Repeating experiment G4 using 1.2 times the observed wind gust variance to create random wind gusts as input to GOTM results in better agreement with the observed T_W compared to $T_{W_{G4}}$ (not shown).

5.3. T_W From LC2015

The estimate of T_W using LC15_stnd and atmospheric forcing from observations (experiment L3) shows overly rapid cooling in the afternoon compared to measured values (gray dashed versus red solid line in Figure 7). T_W relaxes rapidly back to zero because LC15_stnd leaves Regime III (and enters Regime IV) too early. In Regime III of *Large and Caron* [2015], the estimate of the turbulent diffusivity of heat (ν_h) is based on empirical values typical in the presence of internal wave activity and shear instability (section 4.2), consistent with *Price et al*. [1986, 1987], *Schudlich and Price* [1992], and *Smyth et al*. [2013]. A Regime III-like representation of ν_h is appropriate when there is extinction of turbulence [*Kantha and Clayson*, 1994], i.e., when the turbulent kinetic energy is small ($k < k_{\mathrm{lim}} = 10^{-6}$ m^2 s^{-2} in the following). GOTM experiment G1 provides a good estimate of the observed T_W and may provide information on how k evolves in the layer of

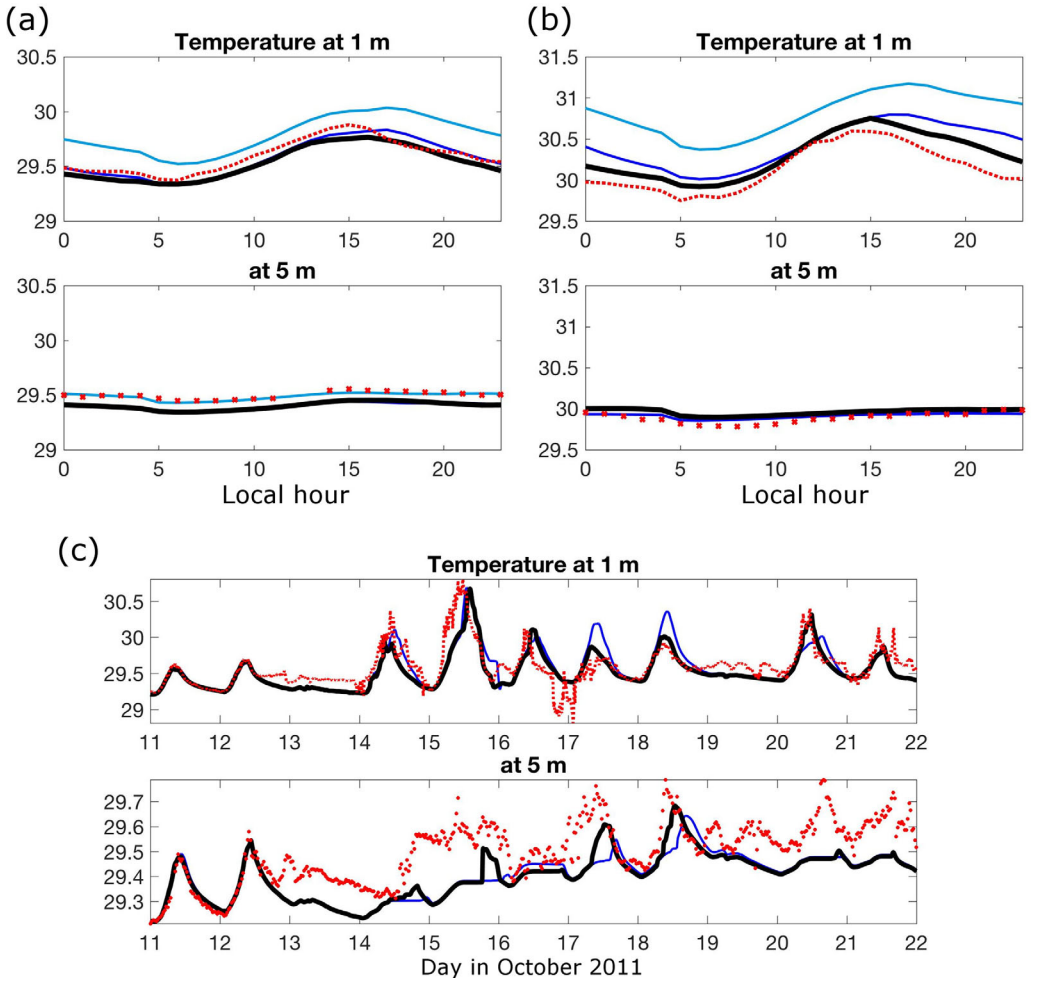

Figure 6. Temperature, °C (a, b) composite day and (c) time series at (top) 1 m and (bottom) 5 m. Figures 6a and 6c are for Period O and Figure 6b for Period N. Temperature is from observations (red line, at 1 m from the RAMA mooring at 0°N, 80.5°E, at 5 m from DYNAMO R/V Revelle) and from simulations G1 (black), G2 (blue), and G5 (light blue). In Figure 6c, tick marks on the horizontal axis correspond to 0500 LST for each day.

interest. Here k decreases rapidly during the formation of the diurnal layer, and increases slowly thereafter (not shown), consistent with LES simulations by *Noh et al.* [2009] and observations (A. Moulin, personal communication, 2016). In *Large and Caron* [2015]'s model, the transition from Regime III to Regime IV should be consistent with k (from G1) becoming larger than k_{lim} in the upper part of the water column. This is not the case for experiment L3: LC15_stnd Regime IV starts (and continues) when most of the upper 10 m of the water column are still characterized by $k < k_{\mathrm{lim}}$ in G1. This is illustrated in Figures 8a and 8b by the presence of green segments (in the top lines) indicating Regime IV at times when turbulence is low (i.e., cross-hatching) through most of the water column.

Using LC2015 with atmospheric forcing from observations as input (experiment L1) improves the estimate of the cooling phase of T_W (Figure 7, gray solid line), delaying the time of the transition between Regimes III and IV. Results are consistent with the vertical profile of k in G1 (e.g., in Figures 8a and 8b, red segments of the bottom line align with upper ocean k overall less than k_{lim}), with Regime IV not occurring on some days. Experiment L1 yields a result closer (than L3) to observations, although r and *rms* are still good for L3 in Period O.

Finally, LC2015 is not very sensitive to wind gusts. In contrast with GOTM, results from LC2015 using winds that are smoothed in time with a 24 h window (experiment L2) are similar to those obtained using the observed winds (gray dots versus gray solid line in Figure 7), with similar r and *rms* (Table 1).

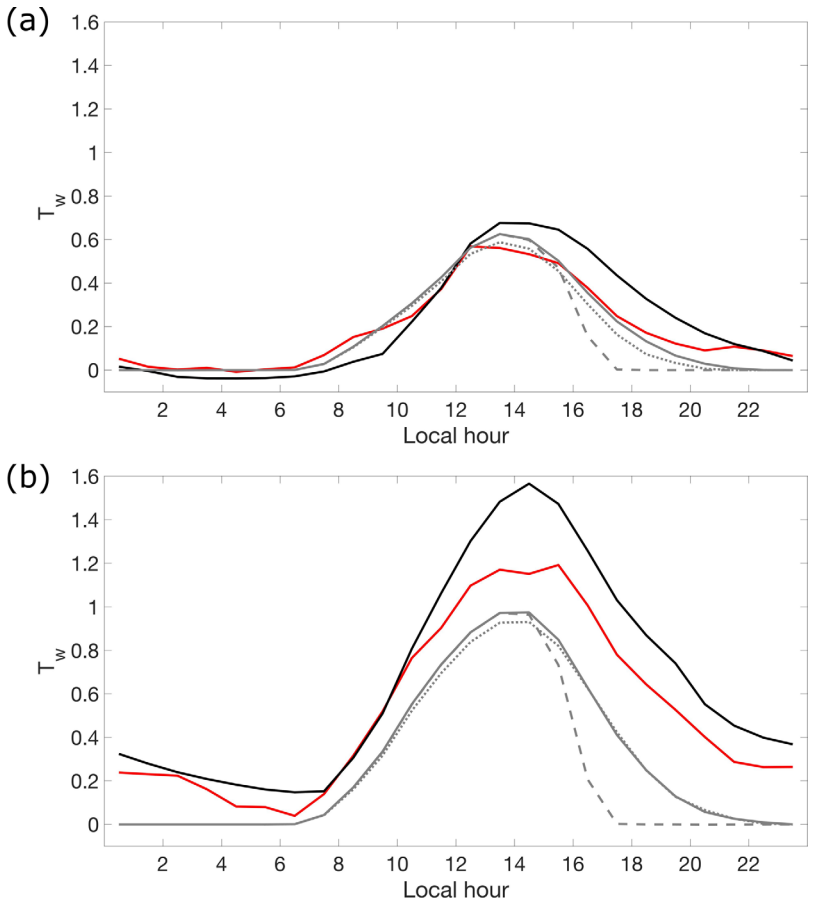

Figure 7. Composite day for T_W (°C) during (a) Period O and (b) Period N. T_W is from DYNAMO R/V Revelle observations (red line), GOTM experiment G1 (black), and *Large and Caron* [2015] experiments L1 (gray), L2 (gray dots), and L3 (gray dashed).

6. Summary and Discussion

Accounting for T_W, the difference between near-surface temperature on a diurnal timescale and ocean temperature at the shallowest level of a climate model (e.g., $z = 10$ m), has the potential to improve simulations of large-scale variability and long-term means in the tropics.

We describe T_W observations around 0°N, 80.5°E during the DYNAMO field campaign, for two periods when the MJO convection is not active at the site (11–21 October, 13–22 November 2011). A diurnal peak in T_W is present on most days, with a composite value of ∼0.55°C for Period O and ∼1.15°C for Period N (Figure 3). The larger diurnal peak in Period N is consistent with a stronger incoming solar radiation and a smaller median wind stress amplitude, hence weaker cooling by nonsolar heat fluxes and weaker turbulent mixing of heat to deeper levels.

Solar forcing is the main driver of diurnal variability [e.g., *Wade et al*., 2011], yet wind gusts modify nonsolar heating and upper ocean mixing. Previous studies showed the importance of high-frequency wind variability for the estimate of nonsolar heat fluxes at the air-sea interface [e.g., *Jabouille et al*., 1996; *Redelsperger et al*., 2000; *Zeng et al*., 2002; *Cronin et al*., 2006]. Here we also consider the role of wind gusts on vertical mixing. The effect of wind gusts on the amplitude of diurnal temperature is stronger through changes in nonsolar heating than through changes in upper ocean mixing. Yet except during nighttime convection, wind gusts regulate how fast surface water is mixed to greater depths when daily mean winds are weak, in a 1-D process model (GOTM). Wind gusts are much stronger than diurnal winds and not only affect the amplitude of the diurnal peak in T_W but also affect the amplitude and timing of diurnal subsurface temperature. The integrated effect of wind gusts over a period of time is essential for a good comparison with observations. Experiments where measured winds are used as input to GOTM provide a good estimate of the observed T_W (experiment G1; Figures 3, 4a, and 5a) and temperature at 1 and 5 m (Figure 6). Experiments where winds are smoothed in time with a 24 h window

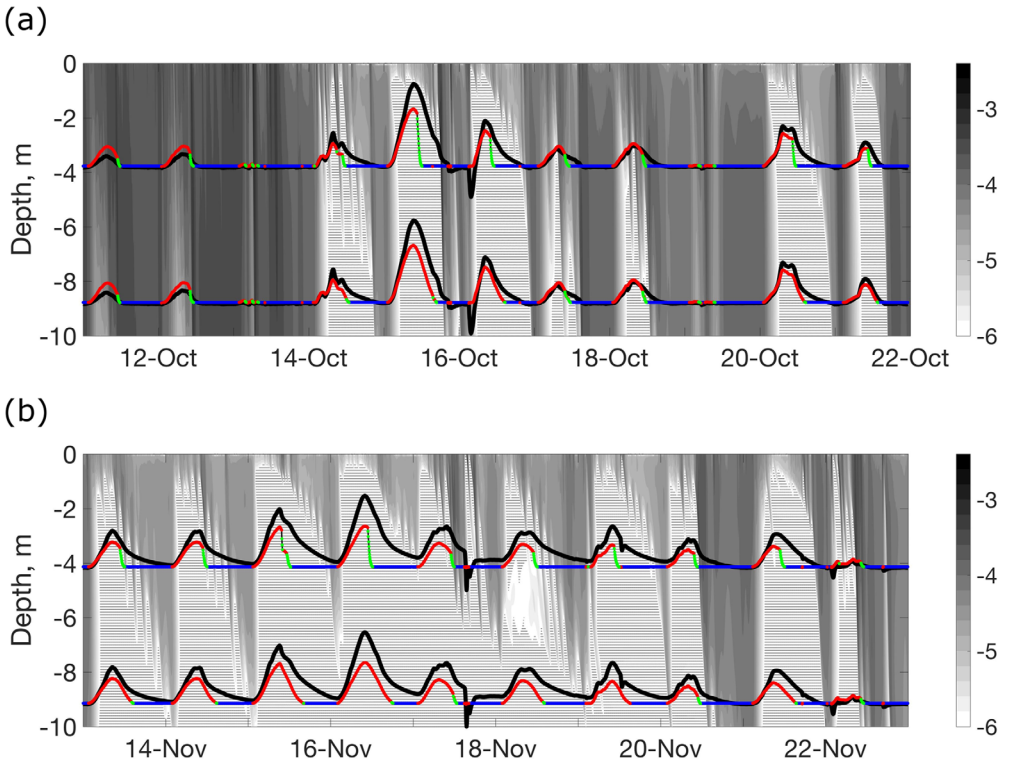

Figure 8. Turbulent kinetic energy (k, $m^2\ s^{-2}$) from experiment G1 (shade) during (a) Period O and (b) Period N. Shaded values are $\log_{10}(k)$. Hatching indicates $k < 10^{-6}\ m^2\ s^{-2}$. In each panel, overlaying solid lines show T_W from experiment G1 (black), L3 (colors, top), and L1 (colors, bottom). Colors indicate Regime I (blue), III (red), and IV (green) in *Large and Caron* [2015]. Tick marks on the horizontal axis correspond to 0500 LST for each day.

yield, instead, a poor comparison with observations, even though observed heat fluxes are used at the air-sea interface and even when the (small) diurnal component of the wind is included. If the estimate of nonsolar heat flux is also based on the smoothed wind, resulting temperatures are even further from observations. Using a 24 h smoothed wind forcing plus stochastic wind gusts as input to GOTM (experiment G4; see section 4.1) yields results that compare well to observations (Figures 3, 4a, and 5a), suggesting the value of a stochastic approach to this problem when the high-frequency component of wind variability is not available, but the statistics of the gusts are known. The 1-D process model in this study suggests that most of the wind gusts are associated with a peak in turbulent kinetic energy at ocean depths of order 1 m, with the strongest events reaching depths of order 10 m. Diurnal variability in wind gusts may also play a role in the tropics (e.g., enhanced convection in the afternoon) but is not detected here.

Vertical resolutions as high as in a 1-D process model like GOTM cannot be implemented within a global climate model, due to limitations in computational resources. Hence, computationally inexpensive diurnal cycling schemes have been proposed to account for T_W diurnal variations in climate simulations, and improve on the estimate of heat fluxes at the air-sea interface. In this study, a variant version of the *Large and Caron* [2015] diurnal cycling scheme (LC2015) provides a good estimate of the observed T_W diurnal variability, improving on the original parameterization (LC15_stnd) by delaying the transition between Regime III (i.e., internal waves and shear-driven mixing) and Regime IV (i.e., strong relaxation of T_W to zero). In LC15_stnd, the transition to Regime IV occurs when convection is initiated near the surface. The required delay is consistent with such convection not reaching immediately the 10 m depth level, and part of the upper 10 m still being stratified. The *Large and Caron* [2015] scheme is not sensitive to wind gusts, and results are similar using observed (experiment L1) or 24 h smoothed (L2) winds to estimate momentum fluxes. This indicates that relevant vertical processes (i.e., the impact of wind gusts on turbulent mixing) may not be well represented even in LC2015. As in GOTM, buoyancy forcing plays a major role in regulating T_W in LC2015, but in order to obtain results that compare well with observations it is also important to choose d, p, and γ parameters (section 4.2) in an appropriate range [*Large and Caron*, 2015]. This is a limitation of

the scheme and makes its application difficult in regions where observations are insufficient to estimate a range for d, p, and γ. At the location of interest here, using $4 \leq d \leq 6$ m, $0.3 \leq p \leq 1.1$, and $0.6 \leq \gamma \leq 1.4$ yields up to ~0.3 °C difference in *rms* and ~1.5 difference in *r*.

In summary, results from LC2015 compare well with observations in this analysis, yet a better representation of how wind gusts regulate mixing (hence T_W diurnal variability) remains desirable. In the current scheme, Regime III shear-driven mixing occurs for most of the daytime (consistent with observations) [e.g., *Sutherland et al*., 2016; *Smyth et al*., 2013], but it acts only to adjust the assumed vertical structure of diurnal temperature. Until the long-term goal of better representing upper ocean processes in climate models can be achieved (e.g., until higher resolution can be implemented in the upper ocean), available data should be used to test the current parameterization and determine appropriate ranges for d, p, and γ at different locations (especially for different latitudes, e.g., where rotation plays a role) [*Price et al*., 1986; *Schudlich and Price*, 1992; *Weller et al*., 2014] and under different wind conditions. The set of optimal parameters are in fact slightly different even here between Period O and Period N (which is characterized by a stronger incoming solar radiation, and a smaller median wind stress amplitude).

Although observations suggest favorable conditions for shear-driven mixing during diurnal stratification (as assumed in Regime III of *Large and Caron* [2015]), high-resolution velocity measurements are required to confirm this [*Sutherland et al*., 2016], and to study the impact of other relevant processes (e.g., Stokes drift) [*Schudlich and Price*, 1992; *Kantha and Clayson*, 2004; *D'Asaro et al*., 2014; *Li et al*., 2016]. For instance, at a site in the Arabian Sea, *Janssen* [2005] finds that buoyancy production and turbulent production by wave breaking are dominant processes for the diurnal cycle, while the Stokes-Coriolis force plays an important role in the deeper layers of the ocean. Also, no sensitivity to Langmuir turbulence is found for the diurnal cycle, consistent with the study (at different sites) of *Kantha and Clayson* [2004].

Finally, long-term wind measurements on a large scale should also be pursued, to observe the statistics of wind gusts and to investigate the role of diurnal winds and wind gusts on upper ocean mixing at different locations (e.g., at higher latitudes) and when more upper ocean processes are modeled. Along with the effort to remedy observational gaps, efforts should be pursued to estimate the diurnal warm layer in new generations of climate models (which will better represent physical processes, e.g., convection) with a goal to improve numerical forecasting of subseasonal, seasonal, and long-term variability. For instance, the LC2015 version of the diurnal cycling scheme should be implemented in a climate model with d, p, and γ parameters based on observations (e.g., spatially varying for better process representation), to investigate how an improved estimate of diurnal SST impacts (for instance) annual SST and mixed-layer depth.

Acknowledgments

This research was supported by NASA, funding NNX14A078G. A.C.S. acknowledges NOAA grant NA14OAR4310276. DYNAMO data were downloaded from the DYNAMO website http://data.eol.ucar.edu/master_list/?project=DYNAMO. Temperature at 10 m depth (T_f) was kindly provided by Jim Moum (Oregon State University) from the Chameleon turbulence profiler [*Moum et al*., 1995]. RAMA mooring data [*McPhaden et al*., 2009] are distributed by the TAO Project Office of NOAA/PMEL (http://www.pmel.noaa.gov/tao/disdel/frames/main.html). Instructions to download and install the General Ocean Turbulence Model (GOTM) source code are available at http://www.gotm.net/index.php, along with detailed information about the GOTM project. Our thanks to William Large (NCAR), Julie Caron (NCAR), and Anton Beljaars (ECMWF) for the many valuable discussions and inputs for this study. Thanks to the two anonymous reviewers for providing valuable feedback.

References

Bernie, D. J., S. J. Woolnough, J. M. Slingo, and E. Guilyardi (2005), Modeling diurnal and intraseasonal variability of the ocean mixed layer, *J. Clim.*, *18*(8), 1190–1202, doi:10.1175/JCLI3319.1.

Bernie, D. J., E. Guilyardi, G. Madec, J. M. Slingo, and S. J. Woolnough (2007), Impact of resolving the diurnal cycle in an ocean–atmosphere GCM: Part 1: A diurnally forced OGCM, *Clim. Dyn.*, *29*(6), 575–590, doi:10.1007/s00382-007-0249-6.

Bernie, D. J., E. Guilyardi, G. Madec, and J. M. Slingo (2008), Impact of resolving the diurnal cycle in an ocean–atmosphere GCM: Part 2: A diurnally coupled CGCM, *Clim. Dyn.*, *31*, 909–925.

Burchard, H., K. Bolding, and M. Villarreal (1999), GOTM—A General Ocean Turbulence Model, Theory, applications and test cases, *Rep. EUR 18745 EN*, 103 pp., Eur. Comm. (Eur. Union), Brussels.

Cronin, M. F., and W. S. Kessler (2009), Near-surface shear flow in the Tropical Pacific cold tongue front, *J. Phys. Oceanogr.*, *39*(5), 1200–1215, doi:10.1175/2008JPO4064.1.

Cronin, M. F., C. W. Fairall, and M. J. McPhaden (2006), An assessment of buoy-derived and numerical weather prediction surface heat fluxes in the Tropical Pacific, *J. Geophys. Res.*, *111*, C06038, doi:10.1029/2005JC003324.

Danabasoglu, G., W. G. Large, J. J. Tribbia, P. R. Gent, B. P. Briegleb, and J. C. McWilliams (2006), Diurnal coupling in the tropical oceans of CCSM3, *J. Clim.*, *19*(11), 2347–2365, doi:10.1175/JCLI3739.1.

D'Asaro, E. A., J. Thomson, A. Y. Shcherbina, R. R. Harcourt, M. F. Cronin, M. A. Hemer, and B. Fox-Kemper (2014), Quantifying upper ocean turbulence driven by surface waves, *Geophys. Res. Lett.*, *41*, 102–107, doi:10.1002/2013GL058193.

Donlon, C., et al. (2007), The global ocean data assimilation experiment high-resolution sea surface temperature pilot project, *Bull. Am. Meteorol. Soc.*, *88*(8), 1197–1213, doi:10.1175/BAMS-88-8-1197.

Fairall, C. W., E. F. Bradley, J. S. Godfrey, G. A. Wick, J. B. Edson, and G. S. Young (1996), Cool-skin and warm-layer effects on sea surface temperature, *J. Geophys. Res.*, *101*(C1), 1295–1308, doi:10.1029/95JC03190.

Gille, S. T. (2012), Diurnal variability of upper ocean temperatures from microwave satellite measurements and Argo profiles, *J. Geophys. Res.*, *117*, C11027, doi:10.1029/2012JC007883.

Hallsworth, S. (2005), Modelling the diurnal variation of sea surface temperature using a one-dimensional ocean turbulence model, PhD thesis, Univ. of Edinburgh, Edinburgh.

Jabouille, P., J. L. Redelsperger, and J. P. Lafore (1996), Modification of surface fluxes by atmospheric convection in the TOGA COARE region, *Mon. Weather Rev.*, *124*(5), 816–837, doi:10.1175/1520-0493(1996)124 < 0816:MOSFBA>2.0.CO;2.

Janssen, P. A. E. M. (2005), Ocean wave effects on the daily cycle in SST, *J. Geophys. Res.*, *117*, C00J32, doi:10.1029/2012JC007943.
Jerlov, N. G. (1968), *Optical Oceanography*, Elsevier. [Available at https://www.elsevier.com/books/optical-oceanography/jerlov/978-0-444-40320-9.]
Kantha, L. H., and C. A. Clayson (1994), An improved mixed layer model for geophysical applications, *J. Geophys. Res.*, *99*(C12), 25,235–25,266, doi:10.1029/94JC02257.
Kantha, L. H., and C. A. Clayson (2004), On the effect of surface gravity waves on mixing in the oceanic mixed layer, *Ocean Modell.*, *6*, 101–124, doi:10.1016/S1463-5003(02)00062-8.
Karagali, I., J. L. Høyer, and C. J. Donlon (2017), Using a 1-D model to reproduce the diurnal variability of SST, *J. Geophys. Res. Oceans*, *122*, 2945–2959, doi:10.1002/2016JC012542.
Kawai, Y., and A. Wada (2007), Diurnal sea surface temperature variation and its impact on the atmosphere and ocean: A review, *J. Oceanogr.*, *63*(5), 721–744, doi:10.1007/s10872-007-0063-0.
Large, W. G., and J. M. Caron (2015), Diurnal cycling of sea surface temperature, salinity, and current in the CESM coupled climate model, *J. Geophys. Res. Oceans*, *120*, 3711–3729, doi:10.1002/2014JC010691.
Li, G., Q. Lin, G. Ni, P. Shen, Y. Fan, L. Huang, and Y. Tan (2012), Vertical patterns of early summer chlorophyll *a* concentration in the Indian Ocean with special reference to the variation of deep chlorophyll maximum, *J. Mar. Biol.*, *2012*, 1–6, doi:10.1155/2012/801248.
Li, Q., A. Webb, B. Fox-Kemper, A. Craig, G. Danabasoglu, W. G. Large, and M. Vertenstein (2016), Langmuir mixing effects on global climate: WAVEWATCH III in CESM, *Ocean Modell.*, *103*, 145–160, doi:10.1016/j.ocemod.2015.07.020.
Matthews, A. J., D. B. Baranowski, K. J. Heywood, P. J. Flatau, and S. Schmidtko (2014), The surface diurnal warm layer in the Indian Ocean during CINDY/DYNAMO, *J. Clim.*, *27*(24), 9101–9122, doi:10.1175/JCLI-D-14-00222.1.
McPhaden, M. J., G. Meyers, K. Ando, Y. Masumoto, V. S. N. Murty, M. Ravichandran, F. Syamsudin, J. Vialard, L. Yu, and W. Yu (2009), Rama: The research moored array for African–Asian–Australian monsoon analysis and prediction, *Bull. Am. Meteorol. Soc.*, *90*(4), 459–480, doi:10.1175/2008BAMS2608.1.
Moum, J. N., M. C. Gregg, R. C. Lien, and M. E. Carr (1995), Comparison of turbulence kinetic energy dissipation rate estimates from two ocean microstructure profilers, *J. Atmos. Oceanic Technol.*, *12*(2), 346–366, doi:10.1175/1520-0426(1995)012 < 0346:COTKED>2.0.CO;2.
Moum, J. N., et al. (2013), Air–sea interactions from westerly wind bursts during the November 2011 MJO in the Indian Ocean, *Bull. Am. Meteorol. Soc.*, *95*(8), 1185–1199, doi:10.1175/BAMS-D-12-00225.1.
Noh, Y., G. Goh, S. Raasch, and M. Gryschka (2009), Formation of a diurnal thermocline in the ocean mixed layer simulated by LES, *J. Phys. Oceanogr.*, *39*(5), 1244–1257, doi:10.1175/2008JPO4032.1.
Paulson, C. A., and J. J. Simpson (1977), Irradiance measurements in the upper ocean, *J. Phys. Oceanogr.*, *7*(6), 952–956, doi:10.1175/1520-0485(1977)007 < 0952:IMITUO>2.0.CO;2.
Pimentel, S., K. Haines, and N. K. Nichols (2008a), Modeling the diurnal variability of sea surface temperatures, *J. Geophys. Res.*, *113*, C11004, doi:10.1029/2007JC004607.
Pimentel, S., K. Haines, and N. K. Nichols (2008b), The assimilation of satellite-derived sea surface temperatures into a diurnal cycle model, *J. Geophys. Res.*, *113*, C09013, doi:10.1029/2007JC004608.
Price, J. F., R. A. Weller, and R. Pinkel (1986), Diurnal cycling: Observations and models of the upper ocean response to diurnal heating, cooling, and wind mixing, *J. Geophys. Res.*, *91*(C7), 8411–8427, doi:10.1029/JC091iC07p08411.
Price, J. F., R. A. Weller, C. M. Bowers, and M. G. Briscoe (1987), Diurnal response of sea surface temperature observed at the long-term upper ocean study (34°N, 70°W) in the Sargasso Sea, *J. Geophys. Res.*, *92*(C13), 14,480–14,490, doi:10.1029/JC092iC13p14480.
Prytherch, J., J. T. Farrar, and R. A. Weller (2013), Moored surface buoy observations of the diurnal warm layer, *J. Geophys. Res. Oceans*, *118*, 4553–4569, doi:10.1002/jgrc.20360.
Redelsperger, J.-L., F. Guichard, and S. Mondon (2000), A parameterization of mesoscale enhancement of surface fluxes for large-scale models, *J. Clim.*, *13*(2), 402–421, doi:10.1175/1520-0442(2000)013 < 0402:APOMEO>2.0.CO;2.
Ruppert, J. H., and R. H. Johnson (2014), Diurnally modulated cumulus moistening in the preonset stage of the Madden–Julian oscillation during DYNAMO, *J. Atmos. Sci.*, *72*(4), 1622–1647, doi:10.1175/JAS-D-14-0218.1.
Schudlich, R. R., and J. F. Price (1992), Diurnal cycles of current, temperature, and turbulent dissipation in a model of the equatorial upper ocean, *J. Geophys. Res.*, *97*(C4), 5409–5422, doi:10.1029/91JC01918.
Seo, H., A. C. Subramanian, A. J. Miller, and N. R. Cavanaugh (2014), Coupled impacts of the diurnal cycle of sea surface temperature on the Madden–Julian oscillation, *J. Clim.*, *27*(22), 8422–8443, doi:10.1175/JCLI-D-14-00141.1.
Smyth, W. D., J. N. Moum, L. Li, and S. A. Thorpe (2013), Diurnal shear instability, the descent of the surface shear layer, and the deep cycle of equatorial turbulence, *J. Phys. Oceanogr.*, *43*(11), 2432–2455, doi:10.1175/JPO-D-13-089.1.
Soloviev, A., and R. Lukas (2006), *The Near-Surface Layer of the Ocean*, pp. 572, Springer, Netherlands.
Stramma, L., P. Cornillon, R. A. Weller, J. F. Price, and M. G. Briscoe (1986), Large diurnal sea surface temperature variability: Satellite and in situ measurements, *J. Phys. Oceanogr.*, *16*(5), 827–837, doi:10.1175/1520-0485(1986)016 < 0827:LDSSTV>2.0.CO;2.
Strutton, P. G., V. J. Coles, R. R. Hood, R. J. Matear, M. J. McPhaden, and H. E. Phillips (2015), Biogeochemical variability in the central equatorial Indian Ocean during the monsoon transition, *Biogeosciences*, *12*(8), 2367–2382, doi:10.5194/bg-12-2367-2015.
Sutherland, G., L. Marié, G. Reverdin, K. H. Christensen, G. Broström, and B. Ward (2016), Enhanced turbulence associated with the diurnal jet in the ocean surface boundary layer, *J. Phys. Oceanogr.*, *46*(10), 3051–3067, doi:10.1175/JPO-D-15-0172.1.
Wade, M., G. Caniaux, Y. duPenhoat, M. Dengler, H. Giordani, and R. Hummels (2011), A one-dimensional modeling study of the diurnal cycle in the equatorial Atlantic at the PIRATA buoys during the EGEE-3 campaign, *Ocean Dyn.*, *61*(1), 1–20, doi:10.1007/s10236-010-0337-8.
Webber, B. G. M., A. J. Matthews, K. J. Heywood, J. Kaiser, and S. Schmidtko (2014), Seaglider observations of equatorial Indian Ocean Rossby waves associated with the Madden-Julian Oscillation, *J. Geophys. Res. Oceans*, *119*, 3714–3731, doi:10.1002/2013JC009657.
Weller, R. A., S. Majumder, and A. Tandon (2014), Diurnal restratification events in the Southeast Pacific trade wind regime, *J. Phys. Oceanogr.*, *44*(9), 2569–2587, doi:10.1175/JPO-D-14-0026.1.
Yoneyama, K., C. Zhang, and C. N. Long (2013), Tracking pulses of the Madden–Julian oscillation, *Bull. Am. Meteorol. Soc.*, *94*(12), 1871–1891, doi:10.1175/BAMS-D-12-00157.1.
Zeng, X., and A. Beljaars (2005), A prognostic scheme of sea surface skin temperature for modeling and data assimilation, *Geophys. Res. Lett.*, *32*, L14605, doi:10.1029/2005GL023030.
Zeng, X., Q. Zhang, D. Johnson, and W.-K. Tao (2002), Parameterization of wind gustiness for the computation of ocean surface fluxes at different spatial scales, *Mon. Weather Rev.*, *130*(8), 2125–2133, doi:10.1175/1520-0493(2002)130 < 2125:POWGFT>2.0.CO;2.